DOI: 10.1002/cvde.200906764

CVD Elaboration of Nanostructured TiO_2-Ag Thin Films with Efficient Antibacterial Properties**

By *Jitti Mungkalasiri*, *Laurent Bedel*, *Fabrice Emieux*, *Jeanne Doré*, *François N. R. Renaud*, *Christos Sarantopoulos*, and *Francis Maury**

Nanostructured TiO_2-Ag composite coatings are deposited by direct liquid injection metal-organic (DLI-MO) CVD at 683 K in a one-step process. Silver pivalate (AgPiv) and titanium tetra-*iso*-propoxide (TTIP) are used as Ag and Ti molecular precursors, respectively. Metallic silver nanoparticles are co-deposited with anatase TiO_2 on stainless steel, glass, and silicon wafers. The silver particles are uniformly embedded in the oxide matrix through the entire film thickness. The influence of the growth conditions, including injection parameters, is investigated on the chemical, physical, and structural characteristics of the coatings as well as on their anti-bacterial activities. The bacterium *Staphylococcus aureus* is employed for anti-bacterial tests. The films are bactericidal, according to the JIS Z 2801 standard test performed in the dark, when they contain less than 1 at.-% of silver. Under UV irradiation they exhibit a photocatalytic activity which decays by increasing the silver content. As a result of this dual functionality, the TiO_2-Ag nanocomposite coatings show promising potentialities as long-term anti-bacterial surfaces since self-cleaning can be achieved periodically under UV light in order to maintain an efficient anti-bacterial activity in the dark or in visible light.

Keywords: Anti-bacterial surfaces, DLI-MOCVD, Nanocomposite coatings, Silver nanoparticles, Titanium dioxide films

1. Introduction

The cost to society of the contamination by pathogen microorganisms in various environments (hospital, air conditioning…) is very high. More importantly, several thousand people die each year because of contamination. Bacteria need solid surfaces for their multiplication and, generally, they develop and form a biofilm. These biofilms, in turn, release into the atmosphere new bacteria which will again contaminate new surfaces. A biofilm is a group of microorganisms on surfaces constituted by complex structures like bacteria, fungus, yeasts, virus, proteins, and polysaccharides for nutriment and protection layers.[1-3] The protection mechanisms of biofilms have been studied in many works.[2,4,5] Removing biofilms from a surface can be done mainly by using physical cleaning,[6,7] but the results are not fully satisfactory.[8] Several hours after these treatments, the surface is re-contaminated by new microorganisms. In order to reduce the risk of contamination and propagation, a surface must exhibit a permanent anti-bacterial activity.

In the literature, various solutions to bacterial contamination of solid surfaces have been proposed. This includes, for instance, conventional chemical or physical surface cleaning as well as high-technology surface treatments such as silver ion implantation,[9,10] silver composite thin films,[11–13] TiO_2 under UV radiation,[14–16] polymer films containing triclosan,[17] quaternary ammonium salts,[18,19] and UV-activated core-shell composite nanoparticles which can be sprayed onto solid surfaces, including the human body.[20–22] Some major disadvantages of the above solutions are the complexity and the high cost of the fabrication process, as well as the use of UV radiation to activate the anti-bacterial behavior when TiO_2 is involved.[21,23]

Triclosan is widely used as anti-microbial agent in various polymers, however it has three major disadvantages: (i) some bacteria resistances have been detected;[24] (ii) it diffuses into the environment, which reduces the long term efficiency of the anti-bacterial effect of the surface; and (iii) it can react with other chemical compounds (e.g., free chlorine in drinking water[25,26]), which can be dangerous to health. Quaternary ammonium salts are also good anti-bacterial agents against some bacteria, but they are

[*] Dr. J. Mungkalasiri, Dr. C. Sarantopoulos, Dr. F. Maury
CIRIMAT, CNRS/INPT/UPS, ENSIACET 4 allée E. Monso, BP 44362, 31432 Toulouse cedex 4 (France)
E-mail: francis.maury@ensiacet.fr

Dr. J. Mungkalasiri, Dr. L. Bedel, Dr. F. Emieux
Laboratoire des Technologies des Surfaces (LTS), DTNM, CEA Grenoble 17, rue des martyrs 38054 Grenoble (France)

J. Doré, Prof. F. N. R. Renaud
Université de Lyon, Nosoco.Tech®, Université Lyon 1, RTI2B 8 avenue Rockefeller, Lyon (France)

[**] The authors thank F.-D. Duminica (CIRMAT, Toulouse) for fruitful discussions in photocatalysis, C. Anglade and M. Jouve (CEA, Grenoble) for technical assistance and A. Di Cara for advice on anti-bacterial tests. This work was supported by CEA, CNRS, and ANR under contract 06-MAPR-0007-01. This article is part of a special section on CVD of Biomaterials.

more efficient against Gram positive bacteria than Gram negative ones, for which they have only a bacteriostatic activity, i.e., a limited anti-bacterial efficiency.[27]

Anatase TiO_2 is a well known photocatalytic material under UV irradiation, and this property is used for self-cleaning applications. In addition to the removal of organic pollutants by photocatalytic oxidation, TiO_2 also exhibits anti-bacterial activity under UV irradiation as reported in many papers.[14-16,23] For indoor applications, however, the continuous use of UV light is dangerous and must be avoided. Attempts to get anti-bacterial behavior under visible light using TiO_2 as a bactericidal material were not convincing, however it is an attractive component combined with an anti-microbial agent for multifunctional properties.

Composite coatings consisting of noble metallic nanoparticles embedded in a matrix are convenient solutions to produce anti-bacterial surfaces without UV activation or chemical agents such as triclosan. For instance, 700 nm thick SiO_2-Ag films were elaborated by a sol-gel process, however to get an anti-bacterial effect of 99.9%, which is the typical target efficiency, the required content of silver was relatively high (Si/Ag = 1:0.25 in the sol).[28] Obviously, this is a disadvantage from an economic point of view. Several researchers have tried to explain the anti-bacterial effect of silver on bacteria.[29-31] An inhibition mechanism was proposed where the cation Ag^+ reacts with proteins by combining the –SH groups of enzymes, which leads to the inactivation of the proteins.[31]

There is a great interest in multifunctional nanocomposite coatings for which advantage of the specific properties of an oxide semiconductor and nanoparticles can be taken. Core/shell TiO_2-$NiFe_2O_4$ composite nanoparticles are an example of this strategy.[20–22] The TiO_2-Ag composite coating is an attractive solution because it combines the anti-bacterial properties of Ag nanoparticles with the photocatalytic activity of the TiO_2 matrix. Furthermore, silver doping can enhance the photocatalytic property of TiO_2 when small quantities are incorporated,[32] or when it is deposited on the surface of the film.[33,34] The processes that have been extensively used for the growth of TiO_2-Ag are sol-gel,[32,33] CVD,[12,34,35] and PVD.[36] The anti-bacterial properties of the TiO_2-Ag nanocomposite coatings were investigated under UV irradiation, but the results could be a combination of the anti-bacterial effect of the TiO_2 surface coating and of direct UV sterilization.[12]

The objective of this work is to develop a large scale, one-step deposition process to produce anti-bacterial surfaces with a long lifetime. Nanostructured TiO_2-Ag composite thin films have been grown for the first time by DLI-MOCVD. In addition to a larger variety of molecular precursors and low deposition temperatures, the DLI-MOCVD process has the usual advantages of the CVD techniques compared to other processes, e.g., a high growth rate and a good control of the reactive gas-phase composition.[37] The choice of the TiO_2 matrix is justified by its physical properties (transparency, photocatalytic effect) and low cost. Silver is one of the reference anti-bacterial metallic agents but it is a quite expensive metal. Consequently, the challenge is to minimize the silver content in the thin films and to keep a high anti-bacterial efficiency of the surfaces without UV light activation and with a good durability. The anti-bacterial activities are discussed as a function of the chemical and structural characteristics of the nanocomposite films in relation to the growth conditions. The anti-bacterial activities are determined against Gram-positive *Staphylococcus aureus*. This bacterium is one of the principal bacteria involved in nosocomial infection problem and one of the most difficult to eliminate.

2. Results and Discussion

2.1. Film Growth Rate

The coatings were deposited in the DLI-MOCVD reactor shown in the Figure 1, and using the deposition conditions reported in Table 1. The thickness of pure TiO_2 thin films increases linearly with the deposition time leading to a typical growth rate of ca. 115 nm min^{-1} (Fig. 2). When the silver precursor is injected simultaneously with TTIP, the growth rate drops to ca. 55 nm min^{-1} even though the same amount of TTIP was injected (frequency 2 Hz). Several hypotheses can explain this behavior: (i) the mixing of the various solvents and precursors in the gas phase may favor a competition between chemical species during the process, for instance in the adsorption step; (ii) the presence of silver nanoparticles on the growing films may block the growth of

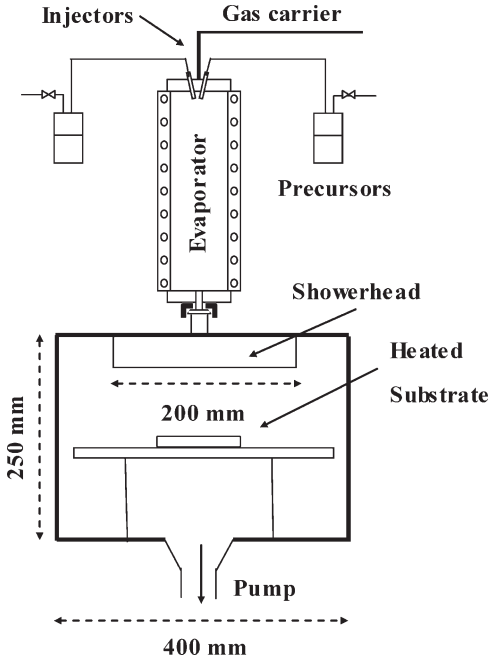

Fig. 1. DLI-MOCVD reactor used for the growth of TiO_2–Ag thin films.

Table 1. Injection parameters used for DLI-MOCVD of TiO_2–Ag nanocomposite films.

Molecular precursor	Solution concentration [mol L^{-1}]	Injection frequency [Hz]	Opening time [ms]	Solvent
TTIP	1	2	2	Xylene
AgPiv	0.1	0.5–6	2	Mesitylene + Propylamine

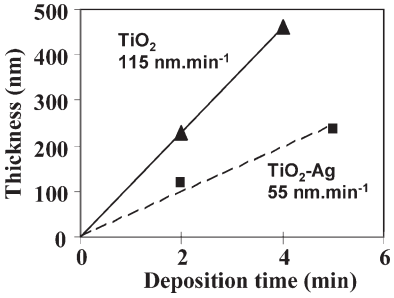

Fig. 2. Influence of the deposition time on the thickness of nanocomposite TiO_2-Ag and pure TiO_2 films grown on Si substrates (the lines are a guide for the eyes).

titanium dioxide crystallites; and (iii) a premature decomposition of TTIP through the showerhead may occur by interaction between both precursors, although the temperature is regulated at a value (473 K) lower than the decomposition temperature of TTIP. The presence of the showerhead improves the gas-phase distribution over the substrate and, consequently, the radial uniformity of the thickness, but it decreases slightly the average value of the thickness. At this stage, further experiments were not undertaken to study the mechanism because our goal was to get uniform thicknesses with a good reproducibility and not to maximize the growth rate.

2.2. Morphology – Structure

Depending on the process parameters, the film thicknesses range from 20 to 300 nm. Surface morphologies and cross-sections of thin films grown on Si show an homogeneous and dense structure (Fig. 3). For low thicknesses, they do not exhibit a columnar growth as frequently observe for MOCVD-produced TiO_2.[38,39] Surface morphology shows a granular structure with typically two populations of aggregates of TiO_2 characterized by an average size of 50 and 150 nm approximately (Fig. 3a). These aggregates consist of nanometric TiO_2 crystallites. The surface roughness (R_a) is typically lower than 30 nm for a thickness of about 300 nm.

The silver particles are too small to be observed by scanning electron microscope (SEM) but they are clearly detected, by transmission electron microscope (TEM), embedded in the TiO_2 matrix (black dots in Fig. 3c). They

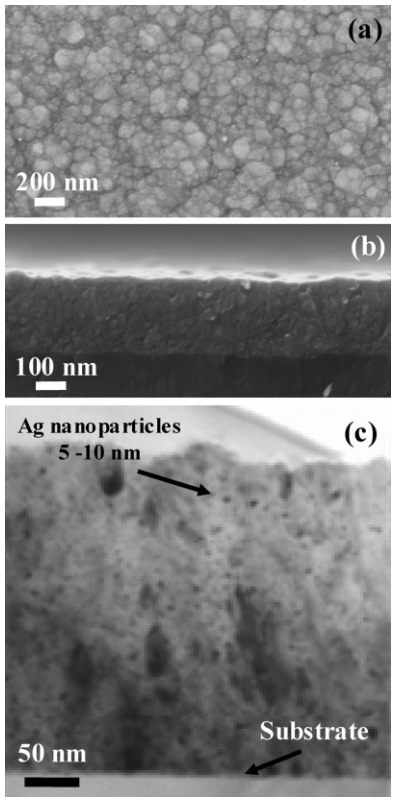

Fig. 3. FEG-SEM images of TiO_2-Ag deposited on a Si substrate; (a) surface, and (b) cross section. (c) Bright field TEM cross-section image showing the Ag nanoparticles.

are uniformly dispersed throughout the thickness of the layer. They exhibit a spherical shape and a small monodisperse size around 5–10 nm. This size is rather smaller than other Ag-matrix nanocomposite films reported in the literature.[13,33]

The X-ray diffraction (XRD) patterns confirm the tetragonal anatase structure of TiO_2 and the cubic close-packed one of silver metal (Fig. 4). Since no evidence was found for preferential orientation of the growth, the relative content of silver can be determined from the XRD intensity

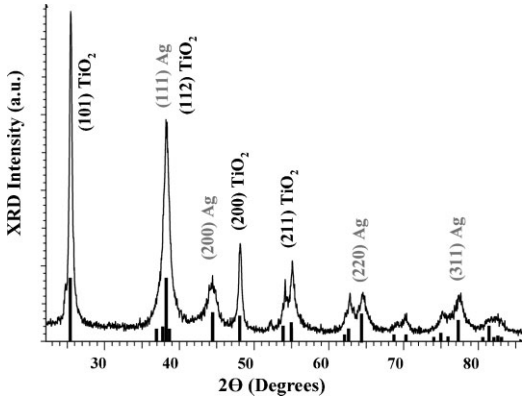

Fig. 4. XRD pattern of a TiO_2-Ag film (grazing incidence 1°) elaborated with AgPiv/TTIP = 0.3.

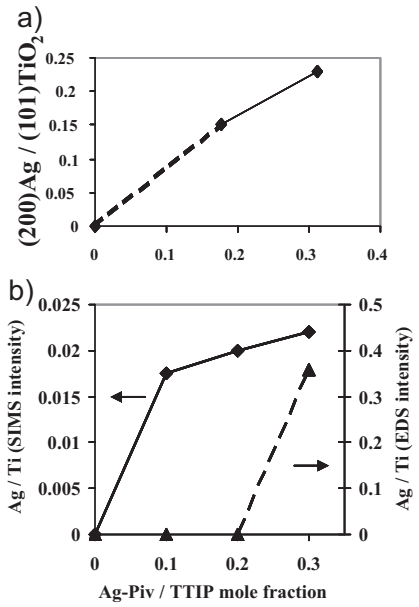

Fig. 5. Influence of the mole fraction ratio AgPiv/TTIP in the reactive gas phase on (a) the (200)Ag/(101)TiO_2 XRD intensity ratio (θ-θ configuration), and (b) the relative Ag content of the films defined as the Ag/Ti intensity ratios determined by SIMS (left Y-axis) and EDS (right Y-axis).

ratio (200)Ag/(101)TiO_2. The (200) Ag peak was preferred to the (111) one because of the overlap with the (112) TiO_2 peak. When the AgPiv/TTIP mole fraction ratio in the gas phase increases (by increasing the injection frequency of AgPiv), the XRD intensity ratio Ag/TiO_2 increases as well, revealing an increase in the silver content of the films (Fig. 5a). As a result, the Ag content of the coatings can be controlled by the mole fraction ratio of the molecular precursors. However, below the AgPiv/TTIP mole fraction ratio of 0.15 (dotted line in Fig. 5a), the intensity of the (200)Ag XRD peak is near the detection limit.

The average crystallite size was calculated after the θ-θ acquisitions using the Scherrer formula for the anatase (101)TiO_2 and (200)Ag XRD peaks. The mean crystallite size is approximately 25 nm and 8 nm, respectively. The average crystallite size of Ag nanoparticles is in very good agreement with the value found by TEM analysis (Fig. 3c). By contrast, the low value found for the TiO_2 crystallite size confirms that the grains observed by SEM are aggregates of these small crystallites. The Ag content has no influence on the mean crystallite size of TiO_2, in agreement with a previous work on TiO_2-Ag.[32]

2.3. Chemical Composition

The low content of silver and the nanometric size of the metallic particles make quantitative chemical analysis difficult. As a result, a relative composition was determined using several techniques including XRD (as above mentioned) and shown in Figure 5a. The intensity ratio Ag/Ti measured by secondary ion mass spectroscopy (SIMS) and X-ray energy dispersive spectroscopy (EDS) is plotted as function of the AgPiv/TTIP mole fraction ratio (Fig. 5b).

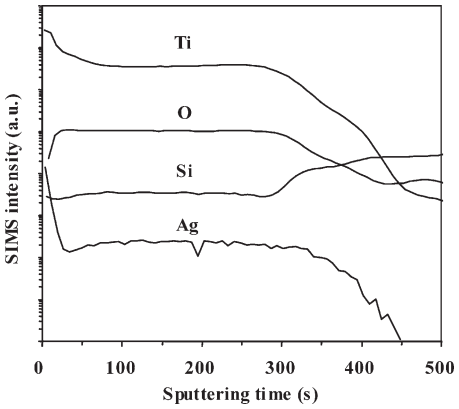

Fig. 6. SIMS depth profiles of a TiO_2-Ag film (60 nm thick) on a Si wafer (the mole fraction ratio AgPiv/TTIP was 0.3).

For low AgPiv mole fractions (AgPiv/TTIP $\leq$ 0.2) the presence of Ag is not detected by EDS analysis. Using a more sensitive technique like SIMS analysis, Ag doping is detected for the lowest AgPiv mole fractions. This technique is currently used for analysis of doping elements in semiconductor materials. X-ray photoelectron spectroscopy (XPS) was also employed to investigate the silver content, but the Ag 3d core level is not detected or its intensity is too low to be extracted from the background for quantification. This confirms that, for most of the samples, Ag content is lower than 1 at.-%. Nevertheless, the silver content increases with the AgPiv mole fraction, as shown in Figure 5. XPS analysis also revealed the carbon content of the films is near the detection limit after Ar^+ sputtering to clean the contamination layer on the surface. This is likely due to the relatively high deposition temperature (683 K) and to the use of oxygen in the reactive gas phase, since both conditions are known to facilitate carbon elimination from the coating to the gas phase in the form of carbon oxides.

Figure 6 presents a SIMS depth profile of a TiO_2-Ag film with a thickness of 60 nm grown on a Si substrate. The signal of silver is constant through the entire film thickness, indicating a uniform distribution of this metallic element. However, we observe a sharp increase near the external surface over about 5 nm, which probably corresponds to secondary effects induced by Ar^+ sputtering due to the surface roughness since no further evidence for silver-rich surface was found.

2.4. Anti-bacterial Properties

The relative Ag content determined by SIMS and EDS was correlated to the anti-bacterial behavior of the thin films (Fig. 7). The anti-bacterial activity of TiO_2-Ag coatings increases strongly for Ag/Ti ratios higher than 0.015 as

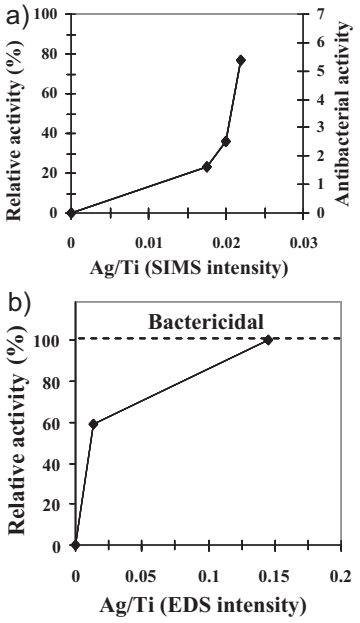

Fig. 7. Relative anti-bacterial activity of TiO_2-Ag films versus the relative Ag content of two series of samples: (a) Films with a low thickness (20 nm) analyzed by SIMS; (b) Film with a thickness higher than 500 nm analyzed by EDS.

determined by SIMS, or 0.01 as determined by EDS. At lower Ag/Ti intensity ratios, there is no or a low activity. Pure TiO_2 films do not exhibit anti-bacterial activity (Ag/Ti = 0 in Fig. 7). It must be recalled that the anti-bacterial tests were performed without UV activation. Clearly, this continuous behavior indicates that the activity is directly dependent on the silver content of the films whatever the thickness since anti-bacterial activity was determined for two series of different film thickness, 20 and 500 nm (Fig. 7). The DLI-MOCVD process allows a good control of the anti-bacterial activity of the surface from low to highly efficient, i.e. bactericidal surfaces.

2.5. Photocatalytic Properties

The photocatalytic activity of TiO_2-Ag films was determined in order to evaluate the possibility to combine the anti-bacterial activity of Ag nanoparticles with the functional properties of the TiO_2 matrix, i.e. the photo-induced self-cleaning behavior. By cleaning periodically the organic contamination of the surface this would improve the durability of the biocidal activity.

The degradation of Orange G dye under UV irradiation in the presence of pure TiO_2 thin films and TiO_2-Ag nanocomposite samples is shown in Figure 8. The photocatalytic efficiency of the samples, defined as the initial decomposition rate of the dye, decreases when the AgPiv/TTIP mole fraction ratio increases. Clearly, pure TiO_2 is the most efficient sample compared to TiO_2-Ag nanocomposite coatings. The low silver incorporation into the film reduces

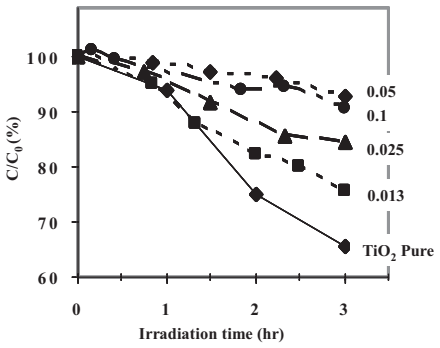

Fig. 8. Photocatalytic decomposition kinetics of an aqueous solution of Orange G (10^{-5} mol L^{-1}) under UV light (365 nm) for TiO_2-Ag samples with various silver contents. The relative Ag content of the films increases with the mole fraction ratio AgPiv/TTIP given for each curves.

the photocatalytic activity. Increasing the silver content above a certain amount (for AgPiv/TTIP > 0.1) leads to the photocatalytic inactivation of the films. No evidence for visible photocatalytic activity was found either for pure TiO_2 or TiO_2-Ag samples.

These results contrast with previous works since a low amount of Ag was found to enhance UV photocatalytic activity of TiO_2 until a certain concentration before decay was observed.[33,34] The difference is that, in our case, the silver nanoparticles are very small (5–10 nm), uniformly dispersed, and embedded in the TiO_2 matrix using a one step process (DLI-MOCVD), while in the literature[33,34] Ag is spread on the surface of TiO_2 by a multistep process. As a result, in our case, the silver nanoparticles contribute predominantly to the increase of the number of defects of the anatase matrix. Indeed, when the silver content increases, the number of Ag nanoparticles increases too without affecting the mean crystallite size of TiO_2. Consequently, the density of defects at the metal-semiconductor interfaces increases which facilitates the electron-hole recombination. Another reason could be the shadowing of the TiO_2 mass by the silver.[33] In this case, the photons are reflected by the silver nanoparticles and cannot reach deeper in the TiO_2 matrix. Thus, TiO_2 films containing small silver amounts are less reactive than pure TiO_2 samples and highly silver-doped films are inactive. Moreover, even though carbon contamination of the films was not found significant by XPS analyses, the use of an additional metal-organic precursor for the co-deposition of silver may induce a higher carbon contamination of the layers than for pure TiO_2 samples. Carbon also acts as a defect and is detrimental to photocatalytic properties, as recently reported for pyrosol TiO_2 films.[40]

In summary, most of the samples exhibit photocatalytic properties under UV light, however the photocatalytic efficiency of the films is decreased by increasing the silver content and, conversely, the anti-bacterial activity is increased. As a result, a compromise has to be found to get simultaneously the dual properties for long term anti-bacterial surfaces, e.g. for AgPiv/TTIP $\approx$ 0.1. The

as-deposited nanocomposite TiO_2-Ag films which exhibit a bactericidal activity (typically for AgPiv/TTIP $\geq$ 0.2) contain a very low Ag amount, near the detection limits of the usual techniques, but this is already too high to maintain a practical photocatalytic activity.

3. Conclusions

TiO_2-Ag coatings were deposited by DLI-MOCVD from TTIP and AgPiv as metal-organic precursors. The physico-chemical and structural features, as well as anti-bacterial and photocatalytic properties, were studied as a function of the AgPiv/TTIP mole fraction ratio in the growth process and, subsequently, the Ag content of the films. This silver amount was found by several analytical techniques (EDS, XRD, XPS, SIMS) to be near the detection limit. TEM observations showed a homogeneous distribution of silver nanoparticles through the entire thickness of the layer. These are monodisperse, 5–10 nm in diameter, whatever the silver content. As a result, bactericidal activity is observed without UV irradiation for very low Ag content (lower than 1 at.-%). Compared to our recent work on TiO_2-Cu composite coatings deposited by a similar process, we deduce that the efficiency of Ag is significantly higher than that of Cu as a biocidal agent since a minimum of 3.5 at-% Cu was necessary to reach a bactericidal behavior.[41]

The nanocomposites TiO_2-Ag coatings can be deposited on various substrates and have promising potential to produce long-lifetime, anti-bacterial surfaces by a CVD process. For instance, for films deposited using AgPiv/TTIP $\approx$ 0.1, a self cleaning can be achieved periodically under UV light owing to the photocatalytic behavior of TiO_2 in order to maintain the anti-bacterial activity in the dark, or in visible light, due to the Ag nanoparticles. On the other hand, even though the dual properties are not optimized for the same coatings, as a result of the constant Ag/TiO_2 ratio through the film thickness, the biocidal activity will be maintained in the case of surface wear caused, for instance, by mechanical abrasion or scratches.

4. Experimental

TiO_2-Ag thin films were deposited in a vertical, low-pressure CVD reactor equipped with a commercial pulsed DLI system connected to a flash vaporization chamber (Fig. 1). The experimental set-up was in three main parts; (i) the vaporization chamber, (ii) a stainless steel deposition reactor including the heating of the substrates, and (iii) the evacuation system. The solutions of precursors were injected through liquid injectors on the top of the vaporization chamber where a flash vaporization occurred. Then the reactive vapor was transported using nitrogen as the carrier gas to the deposition zone. This technique provides higher gas-flow rates than conventional vaporization using bubbler technology.[42] Before reaching the substrates, the gas phase passed through a showerhead in order to distribute the reactive gas phase uniformly onto the surface of the heated substrates. The total pressure during the growth process was automatically controlled using a vacuum pump equipped with an absolute pressure gauge coupled to a throttle valve control system. It was maintained constant at 800 Pa (6 Torr). The substrates (stainless steel 316 L, glass, and Si) were cleaned prior to deposition in an ultrasonic bath containing acetone (15 min), then rinsed with ethanol before being dried under an air stream.

TiO_2-Ag films were grown by injecting simultaneously the two precursors (silver pivalate $(CH_3)_3CC(O)OAg$ (namely AgPiv), and titanium tetra-*iso*-propoxide $Ti\{OCH(CH_3)_2\}_4$ (namely TTIP), dissolved in appropriate solvents) as Ag and Ti sources, respectively. Pure nitrogen (99.9999%) and oxygen (99.9999%) were used as the carrier and reactive gases, respectively ($N_2/O_2 = 9{:}1$). The gas-flow rates were monitored by mass-flow controllers. The AgPiv and TTIP mole fractions were controlled by the injection parameters (frequency, opening time, solution concentration). Two separate injectors were used for the growth of TiO_2–Ag nanocomposite films; one for TTIP and the other for AgPiv. The silver content was varied by controlling the injection frequency keeping constant the other conditions (Table 1).

The temperatures of the evaporator and the showerhead were regulated at 473 K. The reactor wall and the substrate holder were at 523 K and 683 K, respectively. The film thickness was controlled by varying the deposition time.

The films grown on Si wafers were used for the physico-chemical and structural analyses. The crystalline structure of the films and the mean crystallite size were determined by XRD using θ-θ and grazing geometry (Cu Kα). The morphology and thickness of the films were investigated using a SEM (Leo 1530 FEG-SEM) equipped with an EDS analyzer. The size of silver nanoparticles was analyzed using TEM. Electron micro-probe analysis and SIMS were used to determine the relative composition the films and the element distribution through their thickness.

The anti-bacterial properties of TiO_2-Ag films were measured according to the JIS Z 2801 standard using Gram-positive *Staphylococcus aureus* (CIP 4.83). All the tests were performed without UV activation. A bacterial suspension with 3×10^5 CFU per mL (CFU: colony forming unit) was prepared in 1:500 nutrient broth. The samples were cut up (20 mm $\times$ 20 mm each sample). Then, 200 µL of bacterial suspension were put on the samples and covered with the sterile plastic film. The samples were incubated in a chamber for 24 h at 310 K (37 °C) with a relative humidity of about 90%. After incubation, the samples were washed in a universal neutralizer solution in order to collect all bacteria. The recovered suspension was diluted from 10^{-1} to 10^{-4}, and 1 mL of each dilution was brought in a plate (90 mm in diameter) and mixed with 20 mL of the plate count agar (PCA). The plates were incubated for 24 h at 310 K and the numbers of bacteria were counted by the agar plate method. A control sample containing the cell suspension without the nanocomposite coating was also tested. The counts on the three samples (two plates for each) corresponding to a parent sample were averaged. The anti-bacterial activity was calculated using Equation 1.

$$\text{Anti} - \text{bacterial activity} = \log(A/B) \quad (1)$$

A and B are the number of CFU on the surface of the reference and treated samples, respectively. For convenient comparisons between various series, we use also a supplementary definition to qualify the anti-bacterial behavior which is a relative activity given by Equation 2.

$$\text{Relative activity} = \log(A/B) \times 100/\log(A) \quad (2)$$

The meaning of relative activity is as follows; when it is equal to 100% the surface is bactericidal, in the range 0-100% the surface has an anti-bacterial behavior, and at zero the surface is inactive.

The photocatalytic activity of the films was evaluated from the initial decomposition rate of a dye compound in a batch reactor. Films grown on Si substrates (20 mm $\times$ 20 mm) were immersed into an Orange G aqueous solution (10^{-5} mol L^{-1}) and irradiated at 365 nm with a UVA lamp (HPLN Philips 125 W) under a radiance of 1.05 mW cm^{-2}. All solutions were first stirred for 1 h in the dark to assure equilibrium of adsorption with the photocatalyst. The concentration was determined by measuring the absorbance of Orange G at 480 nm, using a UV-vis spectrophotometer. Details are reported elsewhere for UV [38] and visible [43] photocatalytic tests.

[1] J. W. Costerton, P. S. Stewart, E. P. Greenberg, *Science* **1999**, *284*, 1318.

[2] C. A. Fux, J. W. Costerton, P. S. Stewart, P. Stoodley, *Trends Microbiol.* **2005**, *13*, 34.

[3] J. W. Costerton, *Int. J. Anti-microb. Agents* **1999**, *11*, 217.

[4] L. Hall-Stoodley, P. Stoodley, *Curr. Opin. Biotechnol.* **2002**, *13*, 228.

[5] L. R. Johnson, *J. Therm. Biol.* **2008**, *251*, 24.

[6] X. Chen, P. S. Stewart, *Water Res.* **2000**, *34*, 4229.

[7] P. Gilbert, A. J. McBain, A. H. Rickard, *Int. Biodeterior. Biodegrad.* **2003**, *51*, 245.

[8] T. F. Mah, G. A. O'Toole, *Trends Microbiol.* **2001**, *9*, 34.

[9] H. Q. Tang, J. Feng, J. H. Zheng, J. Zhao, *Surf. Coat. Technol.* **2007**, *201*, 5633.

[10] Y. Z. Wan, S. Raman, F. He, Y. Huang, *Vacuum* **2007**, *81*, 1114.

[11] M. Kawashita, S. Tsuneyama, F. Miyaji, T. Kokubo, H. Kozuka, K. Yamamoto, *Biomaterials* **2000**, *21*, 393.

[12] L. A. Brook, P. Evans, H. A. Foster, M. E. Pemble, A. Steele, D. W. Sheel, H. M. Yates, *J. Photochem. Photobiol. A* **2007**, *187*, 53.

[13] H. J. Jeon, S. C. Yi, S. G. Oh, *Biomaterials*, **2003**, *24*, 4921.

[14] Y. Kikuchi, K. Sunada, T. Iyoda, K. Hashimoto, A. Fujishima, *J. Photochem. Photobiol. A* **1997**, *106*, 51.

[15] P. Amezaga-Madrid, R. Silveyra-Morales, L. Cordoba-Fierro, G. V. Nevarez-Moorillon, M. Miki-Yoshida, E. Orrantia-Borunda, F. J. Solis, *J. Photochem. Photobiol. B* **2003**, *70*, 45.

[16] H. M. Coleman, C. P. Marquis, J. A. Scott, S. S. Chin, R. Amal, *Chem. Eng. J.* **2005**, *113*, 55.

[17] W. Zhang, P. K. Chu, J. Ji, Y. Zhang, R. K. Y. Fu, Q. Yan, *Polymer* **2006**, *47*, 931.

[18] M. Marini, M. Bondi, R. Iseppi, M. Toselli, F. Pilati, *Eur. Polym. J.* **2007**, *43*, 3621.

[19] L. Massi, F. Guittard, S. Gribaldi, R. Levy, Y. Duccini, *Int. J. Antimicrob. Agents* **2003**, *21*, 20.

[20] S. Rana, J. Rawat, R. D. K. Misra, *Acta Biomater.* **2005**, *1*, 691.

[21] B. K. Sunkara, R. D. K. Misra, *Acta Biomater.* **2008**, *4*, 273.

[22] S. Rana, J. Rawat, M. M. Sorensson, R. D. K. Misra, *Acta Biomater.* **2006**, *2*, 421.

[23] P. Evans, D. W. Sheel, *Surf. Coat. Technol.* **2007**, *201*, 9319.

[24] S. E. Walsh, J.-Y. Maillard, A. D. Russell, C. E. Catrenich, D. L. Charbonneau, R. G. Bartolo, *J. Hosp. Infect.* **2003**, *55*, 98.

[25] K. L. Rule, V. R. Ebbett, P. J. Vikesland, *Environ. Sci. Technol.* **2005**, *39*, 3176.

[26] E. M. Fiss, K. L. Rule, P. J. Vikesland, *Environ. Sci. Technol.* **2008**, *42*, 976.

[27] *Pharmaceutical codex. Disinfectant and antiseptics* (Ed: W. E. Lund), The Pharmaceutical Press, London 1994, 579.

[28] H. J. Jeon, S. C. Yi, S. G. Oh, *Biomaterials* **2003**, *24*, 4921.

[29] J. S. Kim, E. Kuk, K. N. Yu, J. H. Kim, S. J. Park, H. J. Lee, S. H. Kim, Y. K. Park, Y. H. Park, C. Y. Hwang, Y. K. Kim, Y. S. Lee, D. H. Jeong, M. H. Cho, *Nanomed. Nanotechnol. Biol. Med.* **2007**, *3*, 95.

[30] J. C. Wataha, P. E. Lockwood, A. Schedle, *J. Biomed. Mater. Res. Part A* **2000**, *52*, 360.

[31] Q. L. Feng, J. Wu, G. Q. Chen, F. Z. Cui, T. N. Kim, J. O. Kim, *J. Biomed. Mater. Res.* **2000**, *54*, 662.

[32] C. He, Y. Yu, X. Hu, A. Larbot, *Appl. Surf. Sci.* **2002**, *200*, 239.

[33] I. M. Arabatzis, T. Stergiopoulos, M. C. Bernard, D. Labou, S. G. Neophytides, P. Falaras, *Appl. Catal, B* **2003**, *42*, 187.

[34] X. Zhang, M. Zhou, L. Lei, *Mater. Chem. Phys.* **2005**, *91*, 73.

[35] L. A. Brook, P. Evans, H. A. Foster, M. E. Pemble, D. W. Sheel, A. Steele, H. M. Yates, *Surf. Coat. Technol.* **2007**, *201*, 9373.

[36] S. W. Ryu, E. J. Kim, S. K. Ko, S. H. Hahn, *Mater. Lett.* **2004**, *58*, 582.

[37] J. P. Senateur, R. Madar, F. Weiss, O. Thomas, A. Abrutis, US Patent 5945162

[38] F.-D. Duminica, F. Maury, R. Hausbrand, *Surf. Coat. Technol.* **2007**, *201*, 9304.

[39] F.-D. Duminica, F. Maury, F. Senocq, *Surf. Coat. Technol.* **2004**, *188–189*, 255.

[40] F.-D. Duminica, F. Maury, S. Abisset, *Thin Solid Films*, **2007**, *515*, 7732.

[41] J. Mungkalasiri, L. Bedel, F. Emieux, J. Doré, F. Renaud, F. Maury, *Surf. Coat. Technol.* **2009**, *204*, 887.

[42] F. Maury, F.-D. Duminica, F. Senocq, *Chem. Vap. Deposition* **2007**, *13*, 638.

[43] F.-D. Duminica, F. Maury, R. Hausbrand, *Surf. Coat. Technol.* **2007**, *201*, 9349.